M.R. Flynn and B.R. Sutherland*
University of Alberta, Edmonton, Canada

## 1. INTRODUCTION

Convective storm systems play an important role in the excitation of stratospheric internal gravity waves (IGW). There are three mechanisms for wave generation that have been investigated (Beres *et al.* 2002). "Quasi-stationary forcing" describes the deflection to the mean flow caused by a rising convective element. Because the element acts as a "fluidic" obstacle, this mechanism is similar to IGW excitation by flow over topography. IGW may be generated in the absence of a mean flow through the "mechanical oscillator" or "deep heating" effects. In the former mechanism, IGW excitation results from the oscillatory perturbations to the boundary of a stratified layer due to rising and falling convective elements. By contrast, the source of the forcing through "deep heating" is by fluid expansion from latent heat release.

Here, we propose a fourth, indirect mechanism by which IGW may be excited during deep convection: the perturbation caused by a high-level thunderstorm outflow that travels horizontally near the tropopause. As depicted in Figure 1, examples of such interfacial flows include the tops of tall anvil clouds and high level rope clouds, which are formed by detaching from the leading edge of a convective storm (Simpson 1997).

The efficacy of this mechanism is assessed through a series of laboratory experiments using salt-stratified solutions (Flynn & Sutherland 2003). Although the results only capture Boussinesq dynamics, the experiments can nonetheless be applied to give insight into the atmospheric circumstance described above because the vertical extent over which strong IGW excitation occurs is significantly smaller than the local scale height of the atmosphere.

## 2. EXPERIMENTAL SET-UP

Experiments are performed using a simple lock-release device in which a fluid intrusion of density $\rho_i$ propagates along the interface of a two-layer fluid which has uniform density, $\rho_+$, above the interface and is uniformly stratified fluid below. A schematic of the experimental apparatus is shown in Figure 2. Of interest is the behaviour of the intrusion and the IGW it excites in response to variations in the following experimental parameters: the density difference between the fluid intrusion and the uniform fluid as measured by $\sigma_i = (\rho_i - \rho_+)/\rho_+$; the density jump across the interfacial layer as measured by $\sigma_* = (\rho_* - \rho_+)/\rho_+$ in which $\rho_*$ is the density of the top most layer of stratified fluid; the stratification of the lower layer as measured by $N^2 = -(g/\rho_{00})d\bar{\rho}/dz$ where $d\bar{\rho}/dz$ represents the background density gradient.

As indicated by Figure 2, the lock fluid extended only to the depth of the uniform layer. Thus, no large-scale mean flow of stratified fluid developed as a consequence of releasing the gate. Wave excitation was due solely to the forcing imparted by the fluid intrusion.

Horizontal and vertical time series were used to measure the intrusion's speed of propagation, $v_i$, the depths of penetration into the upper ($h_+$) and

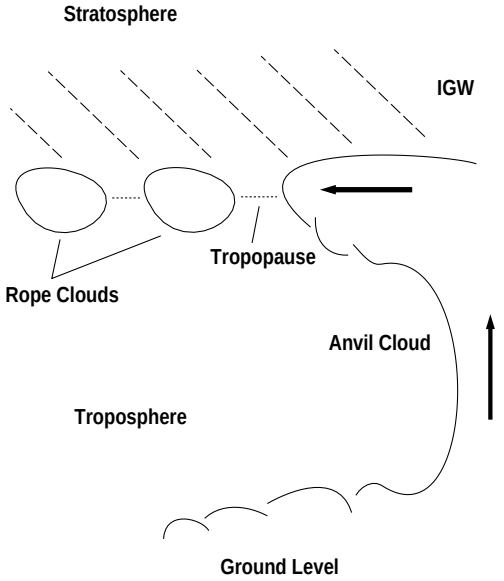


FIGURE 1: Excitation of stratospheric IGW by interfacial outflows.

*Corresponding Author: Dept. Mathematical and Statistical Sciences, U. Alberta, Edmonton, AB T6G 2G1, Canada;
e-mail: bruce.sutherland@ualberta.ca;
web: http://taylor.math.ualberta.ca/~bruce

lower ($h_-$) layers as well as the horizontal extent of the intrusion head, $l_i$. IGW amplitudes were determined using "synthetic schlieren" (Sutherland *et al.* 1999); horizontal wavenumbers and frequencies were computed by applying Fourier transforms to digitized images of the IGW field.

Figure 3 shows a composite vertical time series for that experiment in which $N^2 = 1.17\,\mathrm{s}^{-2}$, $\sigma_* = 0.0037$ and $\sigma_i = 0.0020$. IGW are visualized in the $N_t^2 = d(\Delta N^2)/dt$ field in which $\Delta N^2$ denotes a perturbation to the background buoyancy frequency. Explicitly, $\Delta N^2 = -g/\rho_{00}(d\rho/dz)$ in which $\rho$ is the perturbation density field. Relatively large amplitude waves are observed along the underside of the fluid intrusion. As the IGW propagate downwards, however, their amplitude decreases due to the combined effects of dispersion and viscous attenuation.

## 3. RESULTS

The intrusions behaved as slumping interfacial gravity currents. Unlike the related studies of Amen & Maxworthy (1980) and Maxworthy *et al.* (2002), no resonant interaction was observed between the gravity current and the IGW.

Figure 4 shows $v_i$ (normalized by $\sqrt{\sigma_* g h_i}$ in which $h_i = h_+ + h_-$) as a function of $\zeta_*$ where

$$\zeta_* = \frac{\rho_i - \frac{1}{2}(\rho_* + \rho_+)}{\rho_* - \rho_+}. \qquad (1)$$

Also shown in Figure 4 is a theoretical curve due to the theory of Holyer & Huppert (1980). Their model describes the propagation of a fluid intrusion between layers of uniform density. In the present case, we apply their theoretical model assuming $\rho_{top} = \rho_+$ and $\rho_{bot} = \rho_*$. Furthermore, because the lower layer is stratified in the laboratory experiments, we assume that $H_+ \ll H_-$ where $H_+$ and $H_-$ represent the depths of the upper and lower layers, respectively. Under these conditions, there is good agreement between theory and experiment over a relatively broad range of density space ($-0.50 \leq \zeta_* \lesssim 0.25$). Thereafter, $h_-$ becomes strongly dependent on $N^2$ and the data displays a more significant degree of scatter. The breadth over which strong agreement is noted suggests, however, that in considering the behaviour of the intrusion, the stratification of the lower layer is unimportant

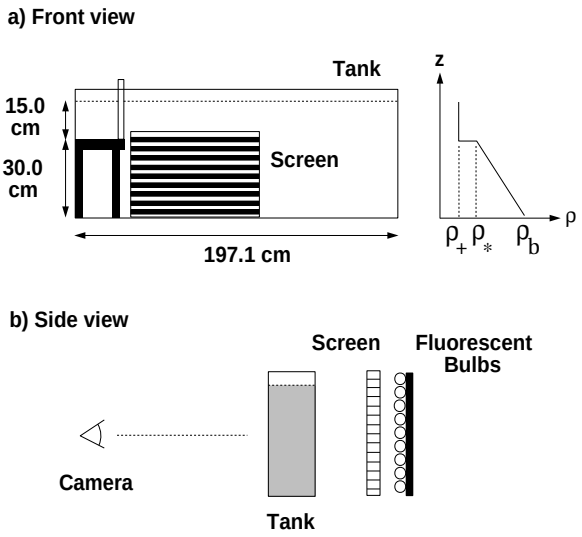


FIGURE 2: (a) Front view of the tank. A schematic representation of the vertical density profile is indicated. (b) Side view of the tank. Figures not to scale.

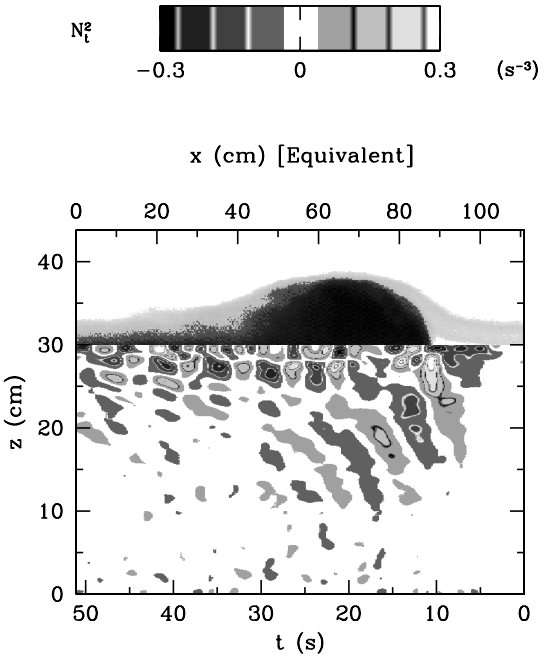


FIGURE 3: Composite time series along a vertical slice one lock-length from the lock release point. IGW amplitudes are indicated by the color bar. Because $v_i$ is constant, the above image is equivalent to a "snapshot" of the wave field with a horizontal dimension as shown.

for a range of density parameters.

The excitation of IGW is due to two related phenomena: the transient collapse of the lock fluid wherein fluid of density $\rho_i$ pushes deeply into the stratified layer, and the forcing imparted by the head of the fluid intrusion as it travels along the interface. Only the latter mechanism is considered in the present study. Generally, wave amplitudes are positively correlated with $h_-$ and hence with $\rho_i$. This is demonstrated by Figure 5 which shows the variation in $A_\xi/\lambda_x$ with $\zeta_*$ where $A_\xi$ is the vertical displacement amplitude and $\lambda_x$, the horizontal wavelength. The relatively high degree of scatter demonstrated by the experimental data is primarily a reflection of the high degree of noise in the wave field (see *e.g.* Figure 3). For $\zeta_* \gtrsim 0.25$, $h_-$ and hence the magnitude of the forcing imparted by the fluid intrusion depends strongly on $N^2$. The wave amplitude is therefore also dependent on $N^2$ in this region of density space.

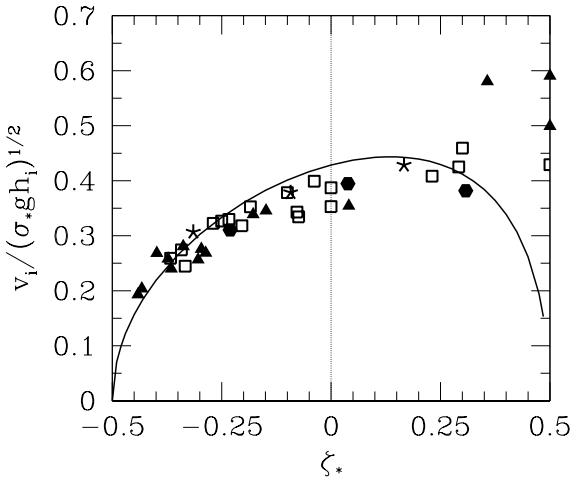


FIGURE 4: Normalized intrusion speed, $v_i/\sqrt{\sigma_* g h_i}$, as a function of $\zeta_*$. Data point types are as follows - closed hexagons: $N^2 = 0.37\,\mathrm{s}^{-2}$; open squares: $N^2 \simeq 0.67\,\mathrm{s}^{-2}$; stars: $N^2 = 0.92\,\mathrm{s}^{-2}$; closed triangles: $N^2 \simeq 1.17\,\mathrm{s}^{-2}$. The solid line indicates the solution predicted by the two-layer model of Holyer & Huppert (1980).

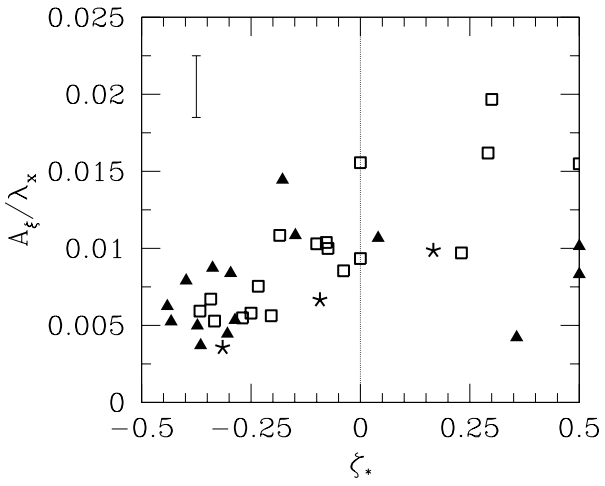


FIGURE 5: Normalized IGW amplitude, $A_\xi/\lambda_x$, as a function of $\zeta_*$. Data point types are as indicated in Figure 4. Typical measurement uncertainties are indicated by the error bar.

In all cases, $A_\xi/\lambda_x$ is notably smaller than the critical amplitudes associated with self-accelerating or overturning instabilities (Sutherland 2000). Wave amplitudes are small in that they do not decelerate the fluid intrusion to any significant degree. Explicitly, letting $\Delta v$ be the change in the intrusion's velocity due to the forcing imparted by the IGW, we find that $\Delta v/v_i$ is typically less than 5%.

Furthermore, the horizontal wavenumber, $k_x$, is inversely proportional to the horizontal extent of the intrusion head, $l_i$. More specifically,

$$k_x = C \cdot \frac{2\pi}{l_i}, \qquad (2)$$

where $C = 1.35 \pm 0.02$. The frequency of wave propagation, $\omega$, is such that the lines of constant phase travel at angles to the vertical, $\Theta = \cos^{-1}(\omega/N)$, of between $41.9^o$ and $52.0^o$. These values are compared with the characteristic angles of wave propagation from four related studies in Table 1 of Flynn & Sutherland (2003).

## 4. DISCUSSION AND CONCLUSIONS

The two-layer theory of Holyer & Huppert (1980) accurately predicts intrusion speeds for $\zeta_* \lesssim 0.25$. IGW excited by the head of the fluid intrusion appear within a narrow band of propagation angles to the vertical, $\Theta$, centered about $47.0^o \pm 2.3^o$. Wave amplitudes generally increase as the density of the intrusion increases.

The goal of the present study is to assess whether interfacial outflows associated with deep convection may excite IGW in the stratosphere that transport significant momentum. The experiments described in §2 consider the mirror reflection of this scenario in which the stratified layer lies beneath the intrusion's plane of propagation. Under the Boussinesq approximation, however, dynamically equivalent results would be obtained if the experiments were con-

ducted with a stratified layer overlying a layer of uniform density.

Numerous idealizations were made in conducting the laboratory experiments. In particular, the atmosphere's vertical density profile is far more complicated than that shown in Figure 2 in that the tropopause is not well represented by a rapid density jump. The results described below are therefore intended to provide insight into wave generation processes and to give crude estimates of the resulting wave momentum fluxes. Additional study is required to confirm their applicability to real flows in the atmosphere.

Figure 6 shows experimentally determined values for $\langle u'w' \rangle / (Nl_i)^2$ as a function of $v_i/\sqrt{\sigma_* g h_i}$ where $\langle u'w' \rangle$ represents the period-averaged Reynolds stress per unit mass. Only those experimental runs for which $\zeta_* \leq 0.25$ are included in this figure. The collapse of the data implies that

$$\frac{\langle u'w' \rangle}{(Nl_i)^2} = 10^{-3.7 \pm 0.6} \left( \frac{v_i}{\sqrt{\sigma_* g h_i}} \right)^{2.9 \pm 0.3} . \quad (3)$$

Selecting $N = 0.02\,\mathrm{s}^{-1}$ a typical value for the stratification of the stratosphere and $l_i = 500\,\mathrm{m}$, a representative length scale for the head of an interfacial outflow, (*e.g.* as visualised by high level rope clouds) equation (3) predicts average values for $\rho_{00} \langle u'w' \rangle$ of between 0.09 and $3\,\mathrm{N/m^2}$. In comparison, Table 1 of Palmer *et al.* (1986) indicates that the average momentum flux associated with topographically excited IGW typically ranges between 0.1 and $1\,\mathrm{N/m^2}$. Although the momentum flux associated with IGW generated by interfacial outflows therefore appears comparable to that of topographically forced IGW, the former mechanism is not expected to be a significant source of IGW outside the sub-tropics where deep convective events occur infrequently. Further study is needed to determine the importance of interfacial outflows relative to the deep heating and obstacle effects and quasi-stationary forcing.

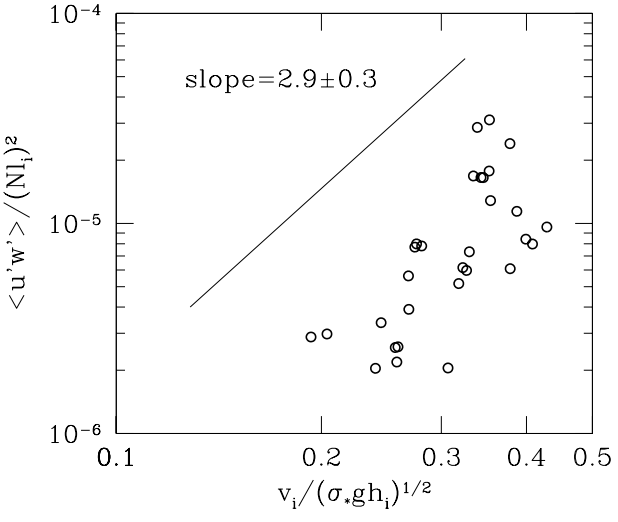


FIGURE 6: Normalized Reynolds stress per unit mass, $\langle u'w' \rangle / (Nl_i)^2$, as a function of $\zeta_*$. The slope of the (vertically offset) best fit line is indicated.

# References


Amen, R. & Maxworthy, T. 1980. The gravitational collapse of a mixed region into a linearly stratified solution. *J. Fluid Mech.*, 96:65–80.

Beres, J. H., Alexander, M. J. & Holton, J. R. 2002. Effects of tropospheric wind shear on the spectrum of convectively generated gravity waves. *J. Atmos. Sci.*, 59:1805–1824.

Flynn, M. R. and Sutherland, B. R. 2003. Fluid intrusions and internal gravity wave generation in stratified media. *J. Fluid Mech.*, in preparation.

Holyer, J. Y. & Huppert, H. E. 1980. Gravity currents entering a two-layer fluid. *J. Fluid Mech.*, 100:739–767.

Maxworthy, T., Leilich, J., Simpson, J. & Meiburg, E. H. 2002. The propagation of a gravity current in a linearly stratified fluid. *J. Fluid Mech.*, 453:371–394.

Palmer, T. N., Shutts, G. J. & Swinbank, R. 1986. Alleviation of a symmetric westerly bias in general circulation and numerical weather prediction models through an orographic gravity drag parametrization. *Quart. J. Roy. Meteor. Soc.*, 112:1001–1039.

Simpson, J. E. 1997. *Gravity Currents in the Environment and the Laboratory*, 2nd Edn. Cambridge University Press, Cambridge, England.

Sutherland, B. R. 2000. Finite-amplitude internal wavepacket dispersion and breaking. *J. Fluid Mech.*, 429:343–380.

Sutherland, B. R., Dalziel, S. B., Hughes, G. O. & Linden, P. F. 1999. Visualisation and measurement of internal waves by "synthetic schlieren". Part 1: Vertically oscillating cylinder. *J. Fluid Mech.*, 390:93–126.